

**Coarse implicit time integration of a  
cellular scale particle model for plant  
tissue deformation**

*Pieter Ghysels      Giovanni Samaey*  
*Paul Van Liedekerke      Engelbert Tijskens*  
*Herman Ramon      Dirk Roose*

*Report TW 562, March 2010*



**Katholieke Universiteit Leuven**  
Department of Computer Science  
Celestijnenlaan 200A – B-3001 Heverlee (Belgium)

# Coarse implicit time integration of a cellular scale particle model for plant tissue deformation

*Pieter Ghysels*      *Giovanni Samaey*  
*Paul Van Liedekerke*      *Engelbert Tijskens*  
*Herman Ramon*      *Dirk Roose*

*Report TW 562, March 2010*

Department of Computer Science, K.U.Leuven

## Abstract

We describe a multiscale method to simulate the deformation of plant tissue. At the cellular scale we use a combination of Smoothed Particle Hydrodynamics (SPH) and discrete elements to model the geometrical structure and basic properties of individual plant cells. At the coarse level, the material is described by the standard continuum approach without explicitly constructing a constitutive equation. Instead, the coarse scale finite element model uses simulations with the fine (cellular) scale model in small subdomains, called Representative Volume Elements (RVEs), to determine the necessary coarse scale variables; such as the stress and the elasticity and viscosity tensors. We present an implicit time integration scheme for the coarse finite element model allowing much larger time steps than possible with explicit methods. Computation of the Cauchy stress from an RVE is straightforward by volume averaging over the RVE. In this work, we use forward finite differencing of the objective Truesdell stress rate to estimate both the fourth order elasticity and viscosity tensors. These tensors are then used to construct the coarse scale stiffness and damping matrices, required for implicit integration.

**Keywords :** multiscale, time integration, implicit, RVE, biological tissue deformation, SPH

**MSC :** Primary : 35B27, Secondary : 35Q70, 92C80.

# Coarse implicit time integration of a cellular scale particle model for plant tissue deformation

P. Ghysels\*, G. Samaey\*, P. Van Liedekerke†  
B. Tijskens†, H. Ramon†, D. Roose\*

March 5, 2010

## Abstract

We describe a multiscale method to simulate the deformation of plant tissue. At the cellular scale we use a combination of Smoothed Particle Hydrodynamics (SPH) and discrete elements to model the geometrical structure and basic properties of individual plant cells. At the coarse level, the material is described by the standard continuum approach without explicitly constructing a constitutive equation. Instead, the coarse scale finite element model uses simulations with the fine (cellular) scale model in small subdomains, called Representative Volume Elements (RVEs), to determine the necessary coarse scale variables; such as the stress and the elasticity and viscosity tensors. We present an implicit time integration scheme for the coarse finite element model allowing much larger time steps than possible with explicit methods. Computation of the Cauchy stress from an RVE is straightforward by volume averaging over the RVE. In this work, we use forward finite differencing of the objective Truesdell stress rate to estimate both the fourth order elasticity and viscosity tensors. These tensors are then used to construct the coarse scale stiffness and damping matrices, required for implicit integration.

## 1 Introduction

Accurate modeling of material behavior requires understanding of the materials properties on different spatial and temporal scales. Over the years, existing coarse scale descriptions such as elasto-visco-plasticity laws have more than proven their success [24]. For almost any type of material behavior, one can find (and tune) an existing constitutive equation to reconstruct experimental observations. However, such models do not give a clear insight in how the underlying fine scale material properties affect the coarse scale behavior. Plant tissue for example, is a material in which properties at the fine (cellular) level influence the coarse tissue behavior in a highly non-trivial way.

In this work, a computational model is considered that appreciates the fine (cellular) scale by explicitly modeling the plant cell walls as thin viscoelastic shells using Discrete Elements (DEM) and the internal of the cells as a viscous fluid using Smoothed Particle Hydrodynamics (SPH). This model is taken from [25], where it is used to investigate the influence of cellular scale plant properties such as cell wall stiffness, cell fluid viscosity and cell geometry on coarse (tissue) scale properties of the material such as tissue rigidity and visco-elasticity. This modeling technique however can hardly be used to compute deformations of *tissue* because of its (associated) computational cost for simulations over large spatio-temporal scales. This paper is devoted to a computational multiscale strategy, based on the concept of Representative Volume Elements (RVEs) [17, 8, 21], that exploits the separation between fine (cellular) and coarse (tissue) scales to

---

\*K.U.Leuven - Department of Computer Science, Celestijnenlaan 200A - bus 2402, B-3001 Heverlee - Belgium, Tel.: +32-16-327700, [pieter.ghysels@cs.kuleuven.be](mailto:pieter.ghysels@cs.kuleuven.be)

†K.U.Leuven - Department of Biosystems, Kasteelpark Arenberg 30 - bus 2456, B-3001 Heverlee - Belgium

significantly reduce the simulation time of the fine scale model, while retaining the cellular scale modeling accuracy and flexibility. The coarse continuum equation, in which the constitutive stress strain relation is not explicitly known, is discretized on the whole domain using standard finite elements, and integrated in time using implicit integration methods. In each quadrature point, we apply a coarse deformation and velocity gradient on an RVE and perform an appropriate fine scale simulation. The required stresses are then evaluated on-the-fly using a stress expression corresponding to the mechanical part of the virial stress.

Explicit time integration for such an RVE based method has already been presented in [11]. The main goal of this paper is to accelerate the coarse scale finite element large deformation model by using appropriate implicit integration methods for stiff systems. This approach requires the coarse stiffness and damping matrices. The main contributions described in this work are hence threefold. First, we introduce a forward finite differencing technique to estimate the anisotropic fourth order elasticity and viscosity tensors, which are then used in the construction of the coarse stiffness and damping matrices. Second, some numerical problems leading to loss of quadratic convergence of the Newton procedure employed in the implicit coarse time-stepper had to be resolved. Quadratic convergence can only be achieved when the Jacobian matrix is sufficiently accurate. Since our estimation of the Jacobian assumes symmetry of the Cauchy stress tensor, it is important to get accurate preservation of linear and angular momentum in the fine scale model. However, the original model as taken from [25] uses the basic Smoothed Particle Hydrodynamics (SPH) equations which do not preserve angular momentum. We therefore had to resort to a different SPH momentum equation, called the nested summation approach in [18], and additionally, a correction to the kernel gradient had to be applied, which was originally proposed by Bonet and Lok [2]. Finally, to solve the fine scale problem in each RVE, i.e. reconstructing the fine scale structure for given coarse deformation and velocity gradients, we use pseudo-transient continuation on a simplified fine scale problem equation. A different procedure to reconstruct the fine scale RVE dynamics using an explicit derivative free iteration is described in [11].

The paper is outlined as follows. In Sect. 2, we discuss the computational fine scale (cellular) model, including a brief description of the SPH and DEM methods for the cell fluid and cell wall respectively. Section 3 describes the fine scale equation to be solved inside the RVEs and the coarse continuum equation. For the coarse equation we briefly discuss the finite element discretization, including the coarse stiffness and damping matrices. Section 4 describes the linearization of the (unknown) constitutive equation and explains how the elasticity and viscosity tensors can be estimated. Section 5 shows the achieved speedup for a numerical example using four different coarse integrators and we conclude the paper in Sect. 6.

## 2 Fine Scale (Cellular) Model

For the fine scale model, describing parenchyma plant cell tissue at the cellular level, we use a Lagrangian mesh-free particle method similar to the model introduced in [25]. The model considers both the solid phase, i.e. the cell wall, and the more fluid-like phase, i.e. the cytoplasm. We first describe the SPH method, used to model the cell fluid, then we discuss the mechanical model for the cell wall, based on the DEM. The reader is referred to [25] for more details.

### 2.1 Cell Fluid

The cell contents is regarded as a simple viscous fluid, which is modeled via smoothed particle hydrodynamics. In SPH [22, 18], the equations of motion of a set of (meso-scale) particles are integrated in time. Associated with each particle is a kernel function. Macroscopic variables of interest, such as pressure, density, velocity, are obtained by interpolation of the particle values by means of their kernel functions. We assume that particle  $i$  is located at position  $\mathbf{x}_i$  and has mass  $m_i$ , density  $\rho_i$ , volume  $V_i$  and velocity  $\mathbf{v}_i$ . The SPH approximation  $\langle f(\mathbf{x}) \rangle$  for a function  $f(\mathbf{x})$

would thus be

$$\langle f(\mathbf{x}) \rangle = \sum_{j=1}^N f(\mathbf{x}_j) W(\mathbf{x} - \mathbf{x}_j, h) V_j, \quad (1)$$

with  $W(\mathbf{x} - \mathbf{x}_j, h)$  the kernel function with smoothing length  $h$ . A popular choice for the kernel function is a cubic spline since it has compact support and its second order derivatives are continuous. It is given by

$$W(\mathbf{x}, h) = \frac{10}{7\pi h^\nu} \begin{cases} 1 - \frac{3}{2}s^2 + \frac{3}{4}s^3, & 0 \leq s \leq 1, \\ \frac{1}{4}(2-s)^3, & 1 \leq s \leq 2, \\ 0, & \text{otherwise,} \end{cases} \quad (2)$$

where  $s = \|\mathbf{x}\|/h$  and  $\nu$  the number of spatial dimensions. We use a constant smoothing length.

In this paper, we restrict ourselves to two dimensions. Then, since  $V_j = m_j/\rho_j$ , the SPH approximation to the density field can be written as

$$\rho(\mathbf{x}) = \sum_{j=1}^N m_j W(\mathbf{x} - \mathbf{x}_j, h), \quad (3)$$

and the density at position  $\mathbf{x}_i$  is evaluated by

$$\rho_i = \sum_{j=1}^N m_j W_i(\mathbf{x}_j), \quad (4)$$

with  $W_i(\mathbf{x}_j) = W(\mathbf{x}_i - \mathbf{x}_j, h)$ . Similarly, the velocity gradient at position  $\mathbf{x}_i$  is approximated in standard SPH using the derivatives of the kernel functions as

$$\nabla \mathbf{v}_i = \sum_{j=1}^N \frac{m_j}{\rho_j} (\mathbf{v}_j - \mathbf{v}_i) \otimes \nabla W_i(\mathbf{x}_j). \quad (5)$$

Since the kernel function is usually written as a function of the distance  $r = |\mathbf{x}_j - \mathbf{x}_i|$  to its center, the gradient can be evaluated as

$$\nabla W_i(\mathbf{x}_j) = \frac{\mathbf{x}_j - \mathbf{x}_i}{|\mathbf{x}_j - \mathbf{x}_i|} \frac{dW}{dr}. \quad (6)$$

The velocity gradient is used to define the rate of deformation tensor  $\mathbf{d}_i$  (at position  $\mathbf{x}_i$ ) as

$$\mathbf{d}_i = \frac{\nabla \mathbf{v}_i + \nabla \mathbf{v}_i^T}{2}, \quad (7)$$

and consecutively the strain rate tensor  $\boldsymbol{\varepsilon}_i$  as

$$\boldsymbol{\varepsilon}_i = 2\mathbf{d}_i - \frac{2}{3}(\mathbf{d}_i : \mathbf{I})\mathbf{I} \quad (8)$$

where  $\mathbf{d} : \mathbf{I} = \text{tr}(\mathbf{d})$  is the double contraction of two second order tensors,  $\mathbf{d}$  and the identity tensor  $\mathbf{I}$ . The viscous stress tensor  $\boldsymbol{\tau}$  is proportional to the strain rate tensor through the viscosity  $\mu$

$$\boldsymbol{\tau}_i = \mu \boldsymbol{\varepsilon}_i. \quad (9)$$

The total stress tensor  $\boldsymbol{\sigma}$  is made up of an isotropic pressure term and the viscous stress  $\boldsymbol{\tau}$  as

$$\boldsymbol{\sigma}_i = -p_i \mathbf{I} + \boldsymbol{\tau}_i, \quad (10)$$

where the pressure is computed from the density through the equation of state

$$p_i = c_s^2 \rho_i \quad (11)$$

with  $c_s$  the speed of sound. From the total stress tensor  $\boldsymbol{\sigma}_i$  at particle  $i$ , the particles acceleration can be computed using the following momentum equation

$$\frac{d\mathbf{v}_i}{dt} = - \sum_{j=1}^N m_j \left( \frac{\boldsymbol{\sigma}_i}{\rho_i^2} + \frac{\boldsymbol{\sigma}_j}{\rho_j^2} \right) \nabla W_i(\mathbf{x}_j). \quad (12)$$

It is important to note that the above formulation for the viscous forces does not preserve angular momentum. In [2], Bonet and Lok propose a correction technique to ensure preservation of angular momentum by enforcing the invariance of a viscous potential energy function with respect to rigid body rotations. This correction also ensures that the gradient of any linear velocity profile is correctly evaluated. The simplest correction proposed by Bonet and Lok involves modifying the kernel gradient used in the evaluation of the velocity gradient  $\nabla \mathbf{v}_i$  in (5) as

$$\tilde{\nabla} W_i(\mathbf{x}_j) = \mathbf{L}_i \nabla W_i(\mathbf{x}_j), \quad (13)$$

where the correction matrix  $\mathbf{L}_i$  of particle  $i$  is defined as

$$\mathbf{L}_i = \left( \sum_{j=1}^N \frac{m_j}{\rho_j} \nabla W_i(\mathbf{x}_j) \otimes (\mathbf{x}_j - \mathbf{x}_i) \right)^{-1}. \quad (14)$$

The velocity gradient  $\nabla \mathbf{v}_i$  at position  $\mathbf{x}_i$  is thus computed as

$$\nabla \mathbf{v}_i = \sum_{j=1}^N \frac{m_j}{\rho_j} (\mathbf{v}_j - \mathbf{v}_i) \otimes \tilde{\nabla} W_i(\mathbf{x}_j) = \sum_{j=1}^N \frac{m_j}{\rho_j} (\mathbf{v}_j - \mathbf{v}_i) \otimes \mathbf{L}_i \nabla W_i(\mathbf{x}_j). \quad (15)$$

## 2.2 Solid Cell Wall

The solid cell wall is considered to be a thin viscoelastic solid which offers no resistance to bending. The wall is represented by particles as in the *discrete element method (DEM)* [6]. In this model, two neighboring cells share one cell wall, making it impossible for two cells to slip along each other or to debond. The masses of the particles in such a combined cell wall are computed from the mass of the combination of the two cell walls and the middle lamella inbetween. Neighboring particles on the cell wall are bonded by a linear elastic spring and a dashpot while a strong repulsive force prevents non-neighboring particles from overlapping. Let  $\mathbf{x}_i$ ,  $\mathbf{v}_i$  and  $m_i$  denote the position, velocity and mass of a particle  $i$ . The relative distance and relative velocity of two particles are denoted by  $\mathbf{x}_{ij} = \mathbf{x}_j - \mathbf{x}_i$  and  $\mathbf{v}_{ij} = \mathbf{v}_j - \mathbf{v}_i$  respectively. The force on particle  $i$  due to the spring connecting particles  $i$  and  $j$  is given by

$$\mathbf{F}_i^S = \left( k_w (l_0 - |\mathbf{x}_{ij}|) - \gamma_c \frac{\mathbf{x}_{ij} \cdot \mathbf{v}_{ij}}{|\mathbf{x}_{ij}|} \right) \frac{\mathbf{x}_{ij}}{|\mathbf{x}_{ij}|} \quad (16)$$

where  $k_w$  is the strength of the harmonic contact,  $l_0$  the initial length of the spring and  $\gamma_c = 2\sqrt{m_i k_w}$  a viscous damping parameter, chosen to get critical damping.

When a particle, DEM or SPH, comes too close to a spring, it will feel a strong repulsive force, which is illustrated in Fig. 1 for two SPH particles  $i$  and  $j$  close to a spring connecting particles 1 and 2. The force on the SPH particle with position  $\mathbf{x}$  is not computed from the individual wall particles but from the spring connecting the two end points with positions  $\mathbf{x}_1$  and  $\mathbf{x}_2$ . For each spring, the point  $\hat{\mathbf{x}}$  on the spring closest to the SPH particle is computed. This point may lie between the two end points, i.e.  $\hat{\mathbf{x}} = c\mathbf{x}_1 + (1-c)\mathbf{x}_2$  or may coincide with  $\mathbf{x}_1$  or  $\mathbf{x}_2$ . We define a repulsive force depending on this shortest distance  $r = |\mathbf{x}_i - \hat{\mathbf{x}}_i|$  of the particle  $i$  to the spring as

$$\mathbf{F}_i^R = \left( \lambda \cos(\alpha) \left( \frac{1}{r^6} - \frac{1}{x_0^6} \right) - 2\sqrt{\frac{6\lambda m_i}{r^7}} \frac{(\mathbf{x}_i - \hat{\mathbf{x}}_i) \cdot (\mathbf{v}_i - \hat{\mathbf{v}}_i)}{r} \right) \frac{\mathbf{x}_i - \hat{\mathbf{x}}_i}{r} \quad (17)$$

for  $r \leq x_0$ , 0 otherwise

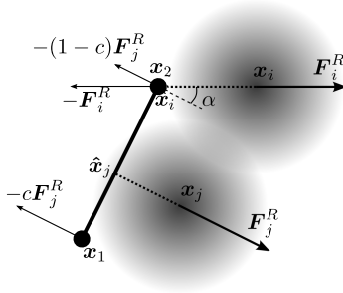


Figure 1: Illustration of the spring-SPH repulsive interaction forces. SPH particles are denoted in gray, wall particles together with their connecting spring are denoted by thick lines.

with  $\lambda$  the strength and  $x_0$  a cutoff distance. The second, velocity dependent term in (17) critically damps the repulsive force for numerical stability. The velocity  $\hat{\mathbf{v}} = c\mathbf{v}_1 + (1-c)\mathbf{v}_2$  is interpolated between the two end points of the spring. In order to get a smoothly varying force, mainly perpendicular to the cell wall, we take into account the angle  $\alpha$ , denoted in Fig. 1. The opposite force  $-\mathbf{F}_i^R = -c\mathbf{F}_i^R - (1-c)\mathbf{F}_i^R$  is divided over the two end points of the spring such that angular momentum is preserved.

### 3 Derivation of a Coarse Continuum Description

In [11] a coarse continuum description for the plant tissue is derived from the discrete fine scale particle model using an extension of the generalized mathematical homogenization technique [9, 4] which also includes the velocity dependence of the inter-particle forces. In this work, we only present the resulting equations at both the fine and coarse scales. For the detailed derivation, the reader is referred to [11].

#### 3.1 Multiple Scale Asymptotic Expansion

The governing equations for the dynamics of the fine scale model, i.e. the combination of SPH and wall DEM particles, are given by Newton's second law of motion

$$m_i \frac{d\mathbf{v}_i}{dt} = \sum_{j=1}^N \mathbf{f}_{ij}(\mathbf{x}_{ij}, \mathbf{v}_{ij}) \quad (18)$$

where the force  $\mathbf{f}_{ij}$  from particle  $j$  acting on particle  $i$  depends on both  $\mathbf{x}_{ij} = \mathbf{x}_j - \mathbf{x}_i$  and  $\mathbf{v}_{ij} = \mathbf{v}_j - \mathbf{v}_i$ , the relative distance and velocity of the particles respectively. The summation in (18) is carried out over all interacting particles. If  $\mathbf{X}_i$  denotes the original position of particle  $i$ , i.e. the position at time  $t = 0$ , then the current position  $\mathbf{x}_i$  can be written as

$$\mathbf{x}_i = \mathbf{X}_i + \mathbf{u}_i \quad (19)$$

with  $\mathbf{u}_i$  the displacement of particle  $i$ .

Two distinct material coordinates to describe both the fine scale and the coarse continuum scale are introduced as follows: let the  $\mathbf{X}$  coordinates denote the coarse scale, at which the fine scale features are invisible, and let the fine features be captured by the coordinates  $\mathbf{Y}$ . Both scales are related by

$$\mathbf{Y} = \frac{\mathbf{X}}{\epsilon} \quad 0 < \epsilon \ll 1, \quad (20)$$

and correspondingly in the current (deformed) configuration  $\mathbf{y} = \mathbf{x}/\epsilon$ . In the same way, we introduce a fast time variable  $\tau$ , related to the standard time  $t$  by

$$\tau = \frac{t}{\epsilon} \quad 0 < \epsilon \ll 1. \quad (21)$$

The assumption of separation in scales leads to a multiple scale asymptotic expansion for the continuum displacement field  $\mathbf{u}(\mathbf{X}, \mathbf{Y}, t, \tau)$  and for the velocity field  $\mathbf{v}(\mathbf{X}, \mathbf{Y}, t, \tau)$  of the form

$$\mathbf{u}(\mathbf{X}, \mathbf{Y}, t, \tau) = \mathbf{u}^0(\mathbf{X}, t) + \epsilon \mathbf{u}^1(\mathbf{X}, \mathbf{Y}, t, \tau) \quad (22)$$

$$\mathbf{v}(\mathbf{X}, \mathbf{Y}, t, \tau) = \mathbf{v}^0(\mathbf{X}, t) + \epsilon \mathbf{v}^1(\mathbf{X}, \mathbf{Y}, t, \tau). \quad (23)$$

The terms  $\mathbf{u}^0(\mathbf{X}, t)$  and  $\mathbf{v}^0(\mathbf{X}, t)$  represent the coarse displacement and velocity fields, which are independent of the fine scale coordinates  $\mathbf{Y}$  and the fast time scale  $\tau$ . The coarse deformation gradient  $\mathbf{F}^0(\mathbf{X}, t)$  and its time derivative  $\dot{\mathbf{F}}^0(\mathbf{X}, t)$  are defined as

$$\mathbf{F}^0(\mathbf{X}, t) = \mathbf{I} + \nabla_{\mathbf{X}} \mathbf{u}^0(\mathbf{X}, t) \quad (24)$$

$$\dot{\mathbf{F}}^0(\mathbf{X}, t) = \nabla_{\mathbf{X}} \mathbf{v}^0(\mathbf{X}, t). \quad (25)$$

Using these notations, Sect. 3.2 describes the fine scale problem, while Sect. 3.3 elaborates on the coarse continuum equation and its finite element discretization.

### 3.2 The Fine Scale Problem

In the coupled multiscale simulations, the problem at the fine scale is given by

$$\begin{aligned} \forall i: \quad m_i \frac{\partial \mathbf{v}_i^1(\mathbf{X}, \mathbf{Y}_i, t, \tau)}{\partial \tau} = & \quad (26) \\ \epsilon \sum_{j \in \text{RVE}} \mathbf{f}_{ij} \left( \mathbf{F}^0(\mathbf{X}, t) \cdot \mathbf{X}_{ij} + \epsilon [\mathbf{u}_j^1 - \mathbf{u}_i^1], \dot{\mathbf{F}}^0(\mathbf{X}, t) \cdot \mathbf{X}_{ij} + \epsilon [\mathbf{v}_j^1 - \mathbf{v}_i^1] \right) \end{aligned}$$

where  $\mathbf{u}_i^1 = \mathbf{u}^1(\mathbf{X}, \mathbf{Y}_i, t, \tau)$  is the fine scale component of the displacement of particle  $i$  at the coarse coordinate  $\mathbf{X} = \mathbf{X}_i$  and fine scale point  $\mathbf{Y}_i$ . Equation (26) corresponds to the original SPH equation, but is defined only on the RVE corresponding to the coarse discretization point  $\mathbf{X}_i$ , together with appropriate boundary conditions. The current position of particle  $i$  is given by the coarse deformation gradient  $\mathbf{F}^0$  applied to the original particle position  $\mathbf{X}_i$  plus an additional fine scale perturbation  $\mathbf{u}_i^1$ . A similar expression holds for the particles velocity. Solving Eq. (26) means finding the fine scale perturbations  $\mathbf{u}_i^1$  and  $\mathbf{v}_i^1$  for all particles. When all fine scale perturbations are ignored, i.e.  $\mathbf{u}_i^1 \equiv \mathbf{0}$  and  $\mathbf{v}_i^1 \equiv \mathbf{0}$ , the deformation is assumed to be constant over the RVE and no internal relaxation of the fine scale structure is allowed. This is called Taylor-Voigt assumption or Cauchy-Born approximation and is only valid for small deformations. Here we will approximate the solution of (26) by ignoring the fine scale perturbations on the particle velocities, i.e. we put  $\mathbf{v}_i^1 \equiv \mathbf{0}$ . This simplifies Eq. (26) to

$$\mathbf{0} = \sum_{j \in \text{RVE}} \mathbf{f}_{ij} \left( \mathbf{F}^0(\mathbf{X}, t) \cdot \mathbf{X}_{ij} + \epsilon [\mathbf{u}_j^1 - \mathbf{u}_i^1], \dot{\mathbf{F}}^0(\mathbf{X}, t) \cdot \mathbf{X}_{ij} \right) \quad \forall i. \quad (27)$$

The four corners of the RVE are given a fixed position and a velocity according to the coarse deformation and velocity gradients respectively by  $\mathbf{x}_{1:4} = \mathbf{F}^0 \cdot \mathbf{X}_{1:4}$  and  $\mathbf{v}_{1:4} = \dot{\mathbf{F}}^0 \cdot \mathbf{X}_{1:4}$ , while on the edges periodic boundary conditions are used. We can efficiently solve for the fine scale perturbations  $\mathbf{u}^1$  from (27) in combination with these periodic boundary conditions using pseudo-transient continuation ( $\Psi$ tc) [16], a well-known technique for the computation of the steady-state solution of a partial differential equation. With Eq. (27) written in the general form  $\mathbf{G}(\mathbf{u}^1) = \mathbf{0}$ , the  $(n+1)$ -st  $\Psi$ tc iteration is written as

$$\mathbf{u}_{n+1}^1 = \mathbf{u}_n^1 - (\delta_n^{-1} \mathbf{I} + \mathbf{G}'(\mathbf{u}_n^1))^{-1} \mathbf{G}(\mathbf{u}_n^1), \quad (28)$$

where the fine scale stiffness matrix  $\mathbf{G}'(\mathbf{u}_n^1)$  is computed using standard finite differences [15]. Initially the fine scale perturbations are set to zero, the initial fine scale state corresponds to the Cauchy-Born approximation. The parameter  $\delta_n$  with  $\delta_0 = 10^{-2}$  is updated after every  $\Psi$ tc iteration by  $\delta_{n+1} = 10\delta_n$ . The iteration (28) is stopped when the step  $\|\mathbf{s}_{n+1} - \mathbf{s}_n\|_2 < 10^{-12}$  or when  $\|\mathbf{G}(\mathbf{s})\|_2 < 10^{-12}$ .

Solving (27) directly might not be feasible for complex fine scale models. In [11], we present a more robust iterative scheme to approximate the solution of (26) without requiring the fine scale Jacobian matrix.

### 3.3 The Coarse Equation

The coarse equation, as it follows from the original dynamical equation (18) by means of the generalized mathematical homogenization technique, corresponds to the classical continuum equation

$$\rho \frac{\partial^2 \mathbf{u}^0(\mathbf{x}, t)}{\partial t^2} = \nabla_{\mathbf{x}} \cdot \langle \boldsymbol{\sigma} \rangle \quad (29)$$

$$\boldsymbol{\sigma}(\mathbf{x}, t, \tau) = \frac{1}{2V_{\text{RVE}}} \sum_{i \in \text{RVE}} \sum_{j \in \text{RVE}} \mathbf{f}_{ij}(\mathbf{x}_{ij}, \mathbf{v}_{ij}) \otimes \mathbf{x}_{ij} \quad (30)$$

with  $\rho = \sum_{j \in \text{RVE}} m_j / V_{\text{RVE}}$  the material density,  $\nabla_{\mathbf{x}} \cdot$  the divergence operator,  $\langle \cdot \rangle$  a time averaging over a fine scale time interval and  $\boldsymbol{\sigma}(\mathbf{x}, t, \tau)$  the Cauchy stress tensor. In the definition of the stress tensor, the inter-particle force depends on  $\mathbf{x}_{ij}$  and  $\mathbf{v}_{ij}$ , as computed by the fine scale model. Note that the definition of the Cauchy stress tensor (30) corresponds to the mechanical part only of the virial stress [26].

In order to solve the governing coarse grained continuum equation (29) with the finite element method, it is first written in its weak form. The domain  $\kappa_t$  is approximated by a set of  $n_{el}$  finite elements  $\kappa_e$ , in which the continuum displacement field  $\mathbf{u} = \mathbf{x} - \mathbf{X}$  is approximated by  $\mathbf{u} \approx \sum_a N_a \tilde{\mathbf{u}}_a$  where  $\tilde{\mathbf{u}}_i$  are the displacements only defined in the discrete nodal positions and  $N_a$  is the shape function corresponding to node  $a$ . The discretization of the coarse continuum equation (29) becomes

$$\mathbf{M} \frac{d^2 \tilde{\mathbf{u}}}{dt^2} = \mathbf{R}(\tilde{\mathbf{u}}, \tilde{\dot{\mathbf{u}}}), \quad \mathbf{R}_a = \sum_{\kappa_e}^{n_{el}} \left( \int_{\kappa_e} \boldsymbol{\sigma} \nabla N_a dv - \int_{\kappa_e} \nabla N_a \mathbf{g} dv \right), \quad (31)$$

with  $\mathbf{g}$  the external body forces and  $\mathbf{M}$  the mass matrix, with elements

$$\mathbf{M}_{ab} = \sum_{\kappa_e}^{n_{el}} \left( \int_{\kappa_e} N_a^T \rho N_b dv \right). \quad (32)$$

This can be written as a system of first order ordinary differential equations (ODEs)

$$\begin{bmatrix} \mathbf{I} & \mathbf{0} \\ \mathbf{0} & \mathbf{M} \end{bmatrix} \frac{d}{dt} \begin{bmatrix} \tilde{\mathbf{u}} \\ \tilde{\dot{\mathbf{u}}} \end{bmatrix} = \begin{bmatrix} \tilde{\dot{\mathbf{u}}} \\ \mathbf{R}(\tilde{\mathbf{u}}, \tilde{\dot{\mathbf{u}}}) \end{bmatrix}. \quad (33)$$

This system of ODEs can be integrated using standard explicit time-stepping algorithms as presented in [11]. However, in this paper we focus on the solution of (33) by an implicit time-stepping algorithm, which generally requires a Jacobian matrix to be supplied to the integration routine. For the system of first order ODEs (33), the Jacobian matrix of the right-hand-side function can be written as

$$\mathbf{J} = \begin{bmatrix} \mathbf{0} & \mathbf{I} \\ -\mathbf{K} & -\mathbf{C} \end{bmatrix} \quad (34)$$

where  $\mathbf{K}$  is called the stiffness matrix and  $\mathbf{C}$  the damping matrix. The stiffness matrix  $\mathbf{K}$  consists of two terms, the initial stress component (first term) and the constitutive component (second term) [3]

$$\mathbf{K}_{ab} = \frac{\partial \mathbf{R}(\tilde{\mathbf{u}}, \tilde{\dot{\mathbf{u}}})}{\partial \tilde{\mathbf{u}}} = \sum_{\kappa_e}^{n_{el}} \left[ \left( \int_{\kappa_e} \nabla N_a \cdot \boldsymbol{\sigma} \nabla N_b dv \right) \mathbf{I} + \int_{\kappa_e} \mathbf{B}_a^T \mathbf{D}^e \mathbf{B}_b dv \right] \quad (35)$$

with  $\mathbf{B}_a$  the standard strain-displacement matrix for two-dimensional displacements

$$\mathbf{B}_a^T = \begin{bmatrix} \partial N_a / \partial x & 0 & \partial N_a / \partial y \\ 0 & \partial N_a / \partial y & \partial N_a / \partial x \end{bmatrix}. \quad (36)$$

The constitutive component of the stiffness matrix depends on the fourth order spatial elasticity tensor  $\mathbf{c}$  (see Sect. 4) through the constitutive matrix  $\mathbf{D}^e$  as

$$\mathbf{D}^e = \frac{1}{2} \begin{bmatrix} 2c_{1111} & 2c_{1122} & c_{1112} + c_{1121} \\ & 2c_{2222} & c_{2212} + c_{2221} \\ \text{sym} & & c_{1212} + c_{1221} \end{bmatrix}. \quad (37)$$

The damping matrix

$$\mathbf{C}_{ab} = \frac{\partial \mathbf{R}(\tilde{\mathbf{u}}, \tilde{\mathbf{u}})}{\partial \tilde{\mathbf{u}}} = \sum_{\kappa_e}^{n_{el}} \left( \int_{\kappa_e} \mathbf{B}_a^T \mathbf{D}^v \mathbf{B}_b dv \right) \quad (38)$$

is based on  $\mathbf{D}^v$ , the viscous constitutive matrix, which is related to the fourth order viscosity tensor  $\boldsymbol{\nu}$  (see Sect. 4) through

$$\mathbf{D}^v = \frac{1}{2} \begin{bmatrix} 2\nu_{1111} & 2\nu_{1122} & \nu_{1112} + \nu_{1121} \\ & 2\nu_{2222} & \nu_{2212} + \nu_{2221} \\ \text{sym} & & \nu_{1212} + \nu_{1221} \end{bmatrix}. \quad (39)$$

The material density  $\rho$  and the Cauchy stress  $\boldsymbol{\sigma}(\tilde{\mathbf{u}}, \tilde{\mathbf{u}})$  at each quadrature point can be computed directly from a fine scale RVE simulation. However, the fourth order spatial elasticity tensor  $\mathbf{c}$  and viscosity tensor  $\boldsymbol{\nu}$  are also material dependent. In Sect. 4, these tensors are defined and a finite difference technique to estimate the elements of the constitutive matrices  $\mathbf{D}^e$  and  $\mathbf{D}^v$  is proposed.

## 4 Linearization

Besides exploiting the separation in spatial scales by only simulating inside the RVEs, it is also possible to exploit the separation in temporal scales. For stability, the time step  $\delta t$  used in the fine scale code is restricted by several criteria which can be summarized as [23]

$$\delta t \leq \min \left( 0.25 \frac{h}{c_s}, 0.25 \min_a \left( \frac{h}{f_a} \right)^{\frac{1}{2}}, 0.125 \frac{h^2}{\nu} \right) \quad (40)$$

with  $h$  the smoothing length,  $c_s$  the speed of sound,  $\nu$  the kinematic viscosity and  $f_a$  the total force on particle  $a$ . Although the coarse system evolves on a much slower timescale, its dynamics might be stiff, hence requiring coarse time steps  $\Delta T$  which may be large compared to the fine scale time step  $\delta t$ , but are still small considering the smooth behavior of the coarse model. In this case, implicit, unconditionally stable methods should be used to allow for larger time-steps.

In the first subsection the rate form of the (unknown) constitutive equation for the viscoelastic fading memory material is formulated based on the objective Truesdell rate. Next, the elasticity and viscosity tensors are estimated using a forward finite difference technique. These approximations are used in the stiffness and damping matrices as introduced in Sect. 3.3.

### 4.1 Rate Formulation of Constitutive Equations

Recall that the spatial velocity field gradient  $\mathbf{l} = \partial \mathbf{v}(\mathbf{x}, t) / \partial \mathbf{x} = \nabla \mathbf{v}$  can be written as  $\mathbf{l} = \dot{\mathbf{F}} \mathbf{F}^{-1}$ , with  $\dot{\mathbf{F}} = \nabla_0 \mathbf{v}$  the time derivative of the deformation gradient, also the velocity gradient with respect to the initial configuration. The symmetric part of the velocity gradient is called the rate

of deformation tensor  $\mathbf{d} = (\mathbf{l} + \mathbf{l}^T)/2$ . As can be observed from the definition of the fine scale problem (26), the constitutive equation takes the general form

$$\boldsymbol{\sigma}(\mathbf{x}, t) = \mathcal{F}\left(\mathbf{x}, \mathbf{F}(t), \dot{\mathbf{F}}(t)\right). \quad (41)$$

After introducing the objective Truesdell rate of the Cauchy stress as

$$\boldsymbol{\sigma}^\circ = \dot{\boldsymbol{\sigma}} - \mathbf{l}\boldsymbol{\sigma} - \boldsymbol{\sigma}\mathbf{l}^T + (\text{tr}\mathbf{l})\boldsymbol{\sigma},$$

with  $\dot{\boldsymbol{\sigma}}$  the time derivative of the Cauchy stress, relation (41) can be rewritten in a linear rate form [3] as

$$\boldsymbol{\sigma}^\circ = \mathbf{c} : \mathbf{d} + \boldsymbol{\nu} : \frac{\mathbf{a}_2}{2} \quad (42)$$

where  $:$  denotes double contraction,  $\mathbf{c}$  is the spatial or Eulerian fourth order elasticity tensor,  $\boldsymbol{\nu}$  is the fourth order spatial viscosity tensor and  $\mathbf{a}_2$  the second Rivlin-Ericksen tensor, defined as

$$\mathbf{a}_2 = \mathbf{l}_2 + \mathbf{l}_2^T + 2\mathbf{l}^T\mathbf{l}, \quad \text{with} \quad \mathbf{l}_2 = \ddot{\mathbf{F}}\mathbf{F}^{-1} = \nabla_0\dot{\mathbf{v}}(\mathbf{x}, t). \quad (43)$$

## 4.2 Finite Difference Approximation

To compute the spatial elasticity and viscosity tensors, we follow the general approach proposed by Miehe [20] for the elasticity tensor, which is based on a forward finite difference approximation and requires only the calculation of stress tensors for slightly perturbed deformation and velocity gradients. The time derivative of the Cauchy stress can be approximated using the forward finite difference formula

$$\begin{aligned} \frac{d\boldsymbol{\sigma}(\mathbf{F}(t), \dot{\mathbf{F}}(t))}{dt} &\approx \frac{\boldsymbol{\sigma}(\mathbf{F}(t + \Delta t), \dot{\mathbf{F}}(t + \Delta t)) - \boldsymbol{\sigma}(\mathbf{F}(t), \dot{\mathbf{F}}(t))}{\Delta t} \\ &\approx \frac{\boldsymbol{\sigma}(\mathbf{F}(t) + \Delta t\dot{\mathbf{F}}(t), \dot{\mathbf{F}}(t) + \Delta t\ddot{\mathbf{F}}(t)) - \boldsymbol{\sigma}(\mathbf{F}(t), \dot{\mathbf{F}}(t))}{\Delta t} \\ &\approx \frac{\boldsymbol{\sigma}(\mathbf{F} + \Delta\mathbf{F}, \dot{\mathbf{F}} + \Delta\dot{\mathbf{F}}) - \boldsymbol{\sigma}(\mathbf{F}, \dot{\mathbf{F}})}{\Delta t} = \frac{\Delta\boldsymbol{\sigma}}{\Delta t} \end{aligned} \quad (44)$$

where we used approximations for the first and second time derivatives of the deformation gradient

$$\dot{\mathbf{F}}(t) \approx \frac{\Delta\mathbf{F}}{\Delta t} = \frac{\mathbf{F}(t + \Delta t) - \mathbf{F}(t)}{\Delta t} \quad \text{and} \quad \ddot{\mathbf{F}}(t) \approx \frac{\Delta\dot{\mathbf{F}}}{\Delta t} = \frac{\dot{\mathbf{F}}(t + \Delta t) - \dot{\mathbf{F}}(t)}{\Delta t} \quad (45)$$

Inserting (44) and (45) in (42) and multiplying with  $\Delta t$  leads to the linearized equation in incremental form

$$\begin{aligned} \Delta\boldsymbol{\sigma} - (\Delta\mathbf{F}\mathbf{F}^{-1})\boldsymbol{\sigma} - \boldsymbol{\sigma}(\Delta\mathbf{F}\mathbf{F}^{-1})^T + \text{tr}(\Delta\mathbf{F}\mathbf{F}^{-1})\boldsymbol{\sigma} = \\ \mathbf{c} : \left( \frac{\Delta\mathbf{F}\mathbf{F}^{-1} + (\Delta\mathbf{F}\mathbf{F}^{-1})^T}{2} \right) \\ + \boldsymbol{\nu} : \left( \frac{\Delta\dot{\mathbf{F}}\mathbf{F}^{-1} + (\Delta\dot{\mathbf{F}}\mathbf{F}^{-1})^T}{2} + (\Delta\mathbf{F}\mathbf{F}^{-1})^T(\Delta\mathbf{F}\mathbf{F}^{-1}) \right). \end{aligned} \quad (46)$$

By taking the perturbations

$$\Delta\mathbf{F}^{(kl)} = \epsilon (\mathbf{e}_k \otimes \mathbf{e}_l) \mathbf{F} \quad \text{and} \quad \Delta\dot{\mathbf{F}} = \mathbf{0} \quad (47)$$

we find an expression for the elements of the spatial constitutive matrix  $\mathbf{D}^e$

$$\begin{aligned} \frac{\mathbf{c}_{ij(kl)} + \mathbf{c}_{ij(lk)}}{2} = \\ \frac{1}{\epsilon} \left[ \Delta\boldsymbol{\sigma}^{(kl)} - (\Delta\mathbf{F}^{(kl)}\mathbf{F}^{-1})\boldsymbol{\sigma} - \boldsymbol{\sigma}(\Delta\mathbf{F}^{(kl)}\mathbf{F}^{-1})^T + \text{tr}(\Delta\mathbf{F}^{(kl)}\mathbf{F}^{-1})\boldsymbol{\sigma} \right]_{ij}. \end{aligned} \quad (48)$$

The viscous part in (46) vanished, because  $\Delta \dot{\mathbf{F}} = \mathbf{0}$  and because we neglected

$$(\Delta \mathbf{F} \mathbf{F}^{-1})^T (\Delta \mathbf{F} \mathbf{F}^{-1}) = O(\epsilon^2) \quad (49)$$

since it is second order in  $\epsilon$ . Now with the perturbations

$$\Delta \mathbf{F} = \mathbf{0} \quad \text{and} \quad \Delta \dot{\mathbf{F}}^{(kl)} = \epsilon_{kl} (\mathbf{e}_k \otimes \mathbf{e}_l) \mathbf{F} \quad (50)$$

we have an expression for the elements of the viscous matrix  $\mathbf{D}^v$

$$\frac{\nu_{ij(kl)} + \nu_{ij(lk)}}{2} = \frac{1}{\epsilon} \Delta \sigma_{ij}^{(kl)}. \quad (51)$$

Evaluating (48) and (51) for different combinations of  $k$  and  $l$  gives the values which are needed to construct the constitutive elastic and viscous matrices  $\mathbf{D}^e$  and  $\mathbf{D}^v$  as defined by (37) and (39) respectively. For plane strain and due to symmetry only three extra stress calculations have to be performed for the elasticity tensor and three for the viscosity tensor.

It is common practice [5, 15] to take the perturbation in a finite difference approximation proportional to the original quantity that must be perturbed. Since the perturbation  $\Delta \mathbf{F}$  on the deformation gradient is already proportional to  $\mathbf{F}$ , we simply choose

$$\epsilon = \sqrt{U} \quad (52)$$

with  $U$  the rounding error. For the perturbations on the velocity gradient we take

$$\epsilon = \sqrt{U} \max(\|\dot{\mathbf{F}}\|_F / \|(\mathbf{e}_k \otimes \mathbf{e}_l) \mathbf{F}\|_F, \dot{F}^{\text{typ}}) \quad (53)$$

where  $\|\cdot\|_F$  denotes the Frobenius norm and  $\dot{F}^{\text{typ}}$  is a typical value for the velocity gradient, which was set to 1. In the multiscale context presented here, the rounding error  $U$  should be comparable to the uncertainty on the stress tensor as computed from the RVE. The value for  $U$  was set equal to the tolerance used in the stopping criterion for the iterative procedure used to reconstruct the fine scale structure, see Sect. 3.2.

## 5 Numerical Results

As a numerical example, we use for the fine scale model the model for plant parenchyma tissue described previously, with the parameters also taken from [25]. A plant cell measures  $25 \times 25 \mu\text{m}$  where each  $25 \mu\text{m}$  side of the cell wall is discretized using 2 springs and the cells are filled with 16 SPH particles. The fluid density  $\rho = 1000 \text{ kg/m}^3$  and the SPH particle mass  $m_i^{\text{SPH}} = 2.7 \cdot 10^{-12} \text{ kg}$  correspond to that of water, while its viscosity was set to  $\mu = 50^{-2} \text{ Pa} \cdot \text{s}$ . To convert the density and viscosity to two-dimensional quantities, we assume a constant thickness of the plant tissue of  $10 \mu\text{m}$ . The SPH smoothing length is set to  $5.5 \mu\text{m}$  and the speed of sound to  $c_s = 100 \mu\text{m/s}$ . The mass of a cell wall particle is  $m_i^{\text{DEM}} = 0.5 \cdot 10^{-12} \text{ kg}$  and the cell wall elastic modulus is set to  $k_w = 4000 \text{ N/m}$ . The repulsive force strength is set to  $\lambda = 5 \cdot 10^5$  and the cutoff distance to  $x_0 = 5 \mu\text{m}$ .

### 5.1 Bending Bar

As a test scenario, a square piece of plant tissue fixed on the left side and bending under the influence of a body force of  $0.2 \mu\text{m}/(\mu\text{s})^2$  pointing downward is considered. The domain,  $400 \times 400 \mu\text{m}$ , consists of  $16 \times 16$  individual square plant cells, stacked in a regular grid, see Fig. 2(left). The same square domain is also discretized using  $4 \times 4$  bilinear quadrilateral finite elements, see Fig. 2(right). Since the fine scale structure is periodic, one period, i.e. one plant cell, is taken as the RVE. The deformation and velocity gradient at each quadrature point are given as input to an RVE centered around the quadrature point. After initialization of the RVE, the stress

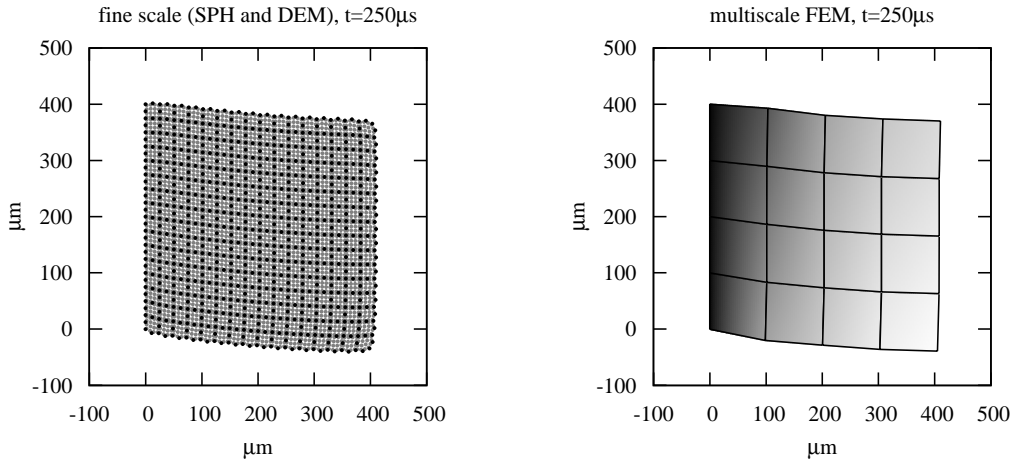


Figure 2: Left: full fine scale,  $16 \times 16$  plant cells, 4096 SPH particles (gray), 833 DEM boundary particles (black); the connecting springs are not shown. Right: coupled multiscale computation, the gray scale denotes the total displacement. Each finite element uses 4+1 quadrature points, so in total  $80 = 4 \times 4 \times 5$  RVEs, one cell each, are used.

tensor is computed using (30). The deviatoric part of the stress tensor  $\boldsymbol{\sigma} - \text{tr}(\boldsymbol{\sigma})/2$  is integrated with a standard  $2 \times 2$  point Gauss quadrature rule, while the hydrostatic pressure  $\text{tr}(\boldsymbol{\sigma})/2$  is under-integrated with a one point Gauss quadrature rule. This approach, called selective reduced integration, improves the elements convergence by reducing volumetric locking [19].

To integrate the coarse finite element model (33), we compare several integration methods. From the CVODE implementation, as available in the SUNDIALS [14] software package, we use two different variable-order variable-step multistep methods: an implicit Adams-Moulton (AM) formula and a Backward Differentiation Formula (BDF). The AM method is used in combination with functional iteration to solve the resulting non-linear system while the BDF method uses Newton iteration. These two methods are also compared to an explicit Runge-Kutta method of order (4)5 due to Dormand and Prince called DOPRI and an implicit Runge-Kutta code of order (5, 9, 13) called RADAU; both Runge-Kutta codes are by Hairer and Wanner [12, 13]. The fine scale system is integrated using the explicit Runge-Kutta DOPRI code. Implicit integration at the fine scale is generally not recommended due to the large number of degrees of freedom. For all integration routines an absolute error tolerance  $10^{-3}$  and a relative tolerance  $10^{-3}$  was used.

Figure 3 shows the vertical displacement of a point in the middle of the right boundary of the domain as a function of time for both the full fine scale model and the coupled multiscale method with the different integration methods. The (rather small) difference between the results for full fine scale and multiscale models is mainly due to the finite size effect of the RVEs [10] and the imperfect reconstruction of the fine scale structure in the RVE. The deviation between the four coarse integrators is within the prescribed tolerances. Only for RADAU the actual steps are marked on the figure, which shows the benefit of the time-step adaptation.

Table 1 compares the number of function evaluations, the number of Jacobian evaluations (if applicable), the number of computed steps and the overall wall clock time of the simulation for the different coarse integrations, as well as for the full fine scale model run. In the fine scale model, a single function evaluation means computing the force on each of the particles for the current particle positions and velocities. A function evaluation for the coarse scale integrator on the other hand, requires a fine scale simulation for every RVE (at each quadrature point) to reconstruct

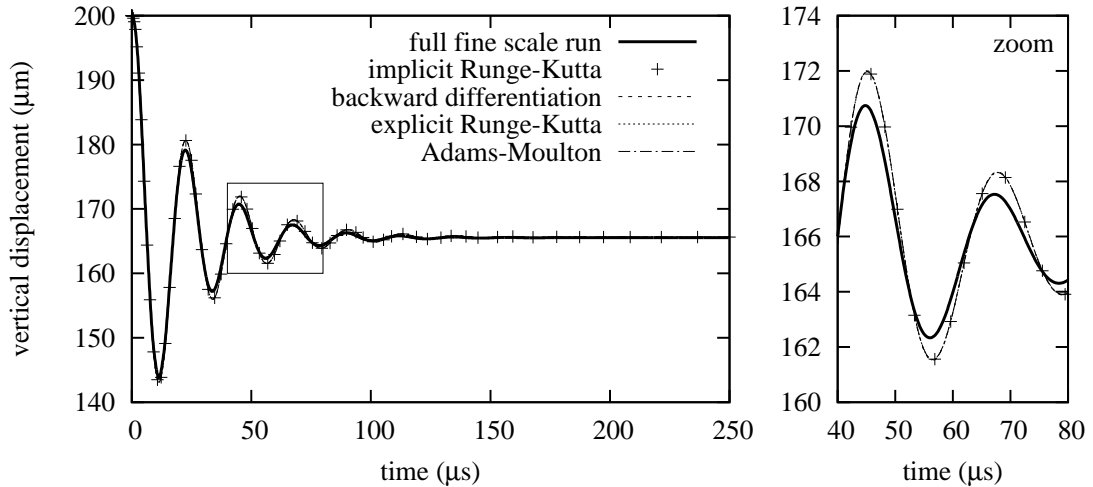


Figure 3: The coarse evolution, represented by its vertical displacement, of a point in the middle of the right side of the domain is plotted as function of time. The difference between multiscale and full fine scale models is small. The differences between the four coarse integrators is within their prescribed tolerances. For the implicit Runge-Kutta RADAU integration, the actual steps are marked.

the fine scale structure inside the RVE for the given coarse scale gradients. Hence a function evaluation for the coarse scale is more expensive than a single fine scale function evaluation, but the coarse scale integrator requires much less evaluations. Note that for larger separation in spatial scales, i.e. a larger domain, the coarse scale function evaluation will become cheaper than a fine scale function evaluation since computations are only performed inside the RVEs. From Table 1, it is clear that the RADAU and BDF methods, which are generally recommended for stiff systems, perform best. Their overall computation time and number of function evaluations are comparable, while the number of computed steps is much higher for the (multistep) BDF method than for RADAU, which is a single step method. The AM method was included in the comparison because it is an implicit method which does not require the Jacobian matrix since it uses functional iteration to solve the resulting nonlinear equation. However, because of the cheap Jacobian estimation, as based on the finite differencing described in Sect. 4, and because the AM method is not recommended for stiff systems, the performance was rather poor compared to RADAU and BDF. For a first comparison between fine and coarse models, we look at the DOPRI method, used both in the fine scale and multiscale simulations. By comparing the number of function evaluations needed in the fine scale and in the coarse scale integration, we have an estimate for the separation in time scales.

## 5.2 Discussion

In the following discussion it is assumed that the computational cost of the multiscale model is mainly determined by the number of fine scale simulations; the overhead of the finite element method is ignored. For instance exploiting the typical structure of the Jacobian matrix in (34) when performing the linear solve is an easy optimization, but does not affect the overall execution time much.

When the user does not supply a routine to compute the Jacobian to the RADAU or BDF codes, both codes will approximate the Jacobian by finite differences, hence only using the right-hand-side function (33). This is significantly less efficient than the approach described in Sect. 4, but it can be convenient for debugging the implementation of the stiffness and damping matrices. Sparse Jacobian matrices can be efficiently estimated using finite differencing when the Curtis-

|                      | fine<br>DOPRI | coarse |       |      |       |
|----------------------|---------------|--------|-------|------|-------|
|                      |               | DOPRI  | RADAU | BDF  | AM    |
| function evaluations | 1911794       | 11024  | 507   | 1652 | 9506  |
| Jacobian evaluations | -             | -      | 60    | 25   | -     |
| accepted steps       | 318630        | 1448   | 66    | 1484 | 5112  |
| computation time     | 6h18m         | 1h39m  | 9m    | 17m  | 1h37m |

Table 1: Quantitative comparison between the different integration methods. Note that a function evaluation for the coarse integrator requires fine scale RVE simulations at all quadrature points. Due to the adaptive step size control and error estimation in the DOPRI and RADAU codes, the number of actually computed steps is slightly larger than the number of accepted steps.

Powell-Reid (CPR) [7] algorithm is used to group columns without overlapping rows with non-zero entries. In the case of a two-dimensional mesh using regular quadrilaterals, a typical row in the stiffness matrix  $\mathbf{K}$  or damping matrix  $\mathbf{C}$  contains 18 (9 point stencil, 2 unknowns per node) non-zero elements. With an ideal grouping of columns, the number of function evaluations needed to estimate the stiffness or damping matrix would still be at least 18. The approach described here only requires 6 extra function evaluations to construct both the stiffness and damping matrices; 3 perturbations on the deformation gradient and 3 on the velocity gradient. The standard finite differencing approach applies perturbations to the nodal positions and velocities, whereas in the approach described here, the perturbations are applied at the quadrature point. A change in nodal position or velocity requires new stress calculations through fine scale simulations for all quadrature points of all elements adjacent to the perturbed node. A perturbation on a deformation gradient at a specific quadrature point only requires an updated stress calculation at that specific quadrature point.

Note that the perturbation  $\Delta\mathbf{F}$  on the deformation gradient  $\mathbf{F}$  is typically very small. The state of the RVE corresponding to the original deformation gradient  $\mathbf{F}$  will be a good estimate for the RVE state corresponding to  $\mathbf{F} + \Delta\mathbf{F}$ . The initialization procedure, the fine scale relaxation, will converge very quickly. For infinitely small deformations, the Cauchy-Born or Taylor-Voigt assumption holds. When we apply this here, i.e. not doing any internal RVE relaxation (thus very cheap Jacobian estimation), the Newton iteration used in the coarse time-stepper only converges linearly. Accordingly, the RADAU method does not take its steps as large as when a more accurate Jacobian is available.

## 6 Conclusions and Outlook

We considered a particle model, a combination of discrete elements and smoothed particle hydrodynamics, which simulates plant tissue; both the viscoelastic solid cell wall and the viscous fluid contained in the cells. In a previous paper [11], a coarse continuum description was derived from the fine scale particle model. Instead of deriving a constitutive relation for the material at the coarse scale, the Cauchy stress tensor is determined on-the-fly from fine scale simulations. In this paper, implicit time integration is used to simulate the transient behavior of the coarse model. Therefore, a coarse scale stiffness and damping matrix had to be constructed. The method proposed here uses a forward finite differencing technique to estimate the spatial elasticity and viscosity tensors, and thus requires only stress calculations. This technique however relies on the symmetry of the Cauchy stress tensor, i.e. the preservation of angular momentum by the fine scale model. Since the basic SPH equations do not satisfy the preservation of angular momentum, a gradient correction had to be used. Removing this last hurdle led to quadratic convergence of the Newton iteration used in the macroscopic integrator.

More realistic problems than the simple bending bar considered here, e.g. on larger domains, will typically have a much larger separation in scales (especially spatial, probably also temporal), hence leading to much larger speedups. However, even for this simple example integrated with

an explicit integrator at the coarse scale, we noticed a significant speedup. This speedup became much larger by recognizing the stiff character of the system and by using the appropriate (implicit) integrators at the coarse scale.

Finally, it might be interesting to have a closer look at the relation between the fine scale initialization procedure as stated here by Eq. (27), which was solved by pseudo-transient continuation, and the constrained-runs initialization procedure discussed in a previous paper [11].

## 7 Acknowledgments

The finite element code was developed using the deal.II C++ library [1]. This paper presents research results of the Belgian Network DYSCO (Dynamical Systems, Control, and Optimization), funded by the Interuniversity Attraction Poles Programme, initiated by the Belgian State, Science Policy Office. The scientific responsibility rests with its authors. This research was supported by the Fund for Scientific Research – Flanders through Research Project (3E060094). GS is a Postdoctoral Fellow of the Research Foundation - Flanders (FWO).

## References

- [1] W. Bangerth, R. Hartmann, and G. Kanschat. deal.II — a general-purpose object-oriented finite element library. *ACM Transactions on Mathematical Software*, 33(4), 2007.
- [2] J. Bonet and T. S. L. Lok. Variational and momentum preservation aspects of smooth particle hydrodynamic formulations. *Computer Methods in Applied Mechanics and Engineering*, 180(1-2):97–115, 1999.
- [3] J. Bonet and R. D. Wood. *Nonlinear continuum mechanics for finite element analysis*. Cambridge University Press, 1997.
- [4] W. Chen and J. Fish. A mathematical homogenization perspective of virial stress. *International Journal for Numerical Methods in Engineering*, 67:189–207, 2006.
- [5] A. R. Conn, N. I. M. Gould, and P. L. Toint. *Trust-region methods*. SIAM, 2000.
- [6] P. A. Cundall and O. D. L. Strack. A discrete numerical model for granular assemblies. *Geotechnique*, 29(1):47–65, 1979.
- [7] A. R. Curtis, M. J. D. Powell, and J. K. Reid. On the estimation of sparse Jacobian matrices. *J. Inst. Math. Appl*, 13:117–119, 1974.
- [8] F. Feyel and J. L. Chaboche. FE2 multiscale approach for modelling the elastoviscoplastic behaviour of long fibre SiC/Ti composite materials. *Computer Methods in Applied Mechanics and Engineering*, 183(3):309–330, 2000.
- [9] J. Fish, W. Chen, and R. Li. Generalized mathematical homogenization of atomistic media at finite temperatures in three dimensions. *Computer Methods in Applied Mechanics and Engineering*, 196(4-6):908 – 922, 2007.
- [10] P. Ghysels, G. Samaey, E. Tijskens, P. Van Liedekerke, H. Ramon, and D. Roose. Multi-scale simulation of plant tissue deformation using a model for individual cell mechanics. *Phys. Biol*, 6(016009):016009, 2009.
- [11] P. Ghysels, G. Samaey, P. Van Liedekerke, E. Tijskens, H. Ramon, and D. Roose. Multi-scale modeling of viscoelastic plant tissue. *Accepted in International Journal for Multiscale Computational Engineering*, 2009.
- [12] E. Hairer, S. P. Nørsett, and G. Wanner. *Solving ordinary differential equations I: nonstiff problems*. Springer, 1993.

- [13] E. Hairer, S. P. Nørsett, and G. Wanner. *Solving ordinary differential equations II: stiff and differential-algebraic problems*. Springer, 1993.
- [14] A. C. Hindmarsh, P. N. Brown, K. E. Grant, S. L. Lee, R. Serban, D. E. Shumaker, and C. S. Woodward. SUNDIALS: Suite of nonlinear and differential/algebraic equation solvers. *ACM Transactions on Mathematical Software (TOMS)*, 31(3):363–396, 2005.
- [15] C. T. Kelley. *Solving nonlinear equations with Newton’s method*. Fundamentals of Algorithms. SIAM, Philadelphia, 2003.
- [16] C. T. Kelley and D. E. Keyes. Convergence analysis of pseudo-transient continuation. *SIAM Journal on Numerical Analysis*, 35(2):508–523, 1998.
- [17] V. Kouznetsova, W. A. M. Brekelmans, and F. P. T. Baaijens. An approach to micro-macro modeling of heterogeneous materials. *Computational Mechanics*, 27:37–48, 2001.
- [18] M. B. Liu. *Smoothed particle hydrodynamics: a meshfree particle method*. World Scientific, 2003.
- [19] D. S. Malkus and T. J. R. Hughes. Mixed finite element methods - Reduced and selective integration techniques - A unification of concepts. *Computer Methods in Applied Mechanics and Engineering*, 15:63–81, 1978.
- [20] C. Miehe. Numerical computation of algorithmic (consistent) tangent moduli in large-strain computational inelasticity. *Computer Methods in Applied Mechanics and Engineering*, 134:223–240, 1996.
- [21] C. Miehe, J. Schroder, and J. Schotte. Computational homogenization analysis in finite plasticity simulation of texture development in polycrystalline materials. *Computer Methods in Applied Mechanics and Engineering*, 171(3-4):387–418, 1999.
- [22] J. J. Monaghan. Smoothed particle hydrodynamics. *Annual review of astronomy and astrophysics*, 30(1):543–574, 1992.
- [23] J. P. Morris, P. J. Fox, and Y. Zhu. Modeling low Reynolds number incompressible flows using SPH. *Journal of Computational Physics*, 136(1):214–226, 1997.
- [24] J. C. Simo and T. J. R. Hughes. *Computational inelasticity*. Springer New York, 1998.
- [25] P. Van Liedekerke, E. Tijskens, H. Ramon, P. Ghysels, G. Samaey, and D. Roose. A particle based model to simulate plant cells dynamics. In D. Le Touzé, editor, *Proceedings of the 4th international SPHERIC workshop, Nantes, France*, pages 209–216, 2009.
- [26] M. Zhou. A new look at the atomic level virial stress: on continuum-molecular system equivalence. *Proceedings: Mathematical, Physical & Engineering Sciences*, 459:2347–2392, 2003.